 doi:10.20944/preprints202209.0392.v1

Micro-particles of high entropy alloys made by laser induced forward transfer

Molong Han,[1] Ashok Meghwal,[2, a)] Soon Hock Ng,[1, b)] Daniel Smith,[1] Haoran Mu,[1] Tomas Katkus,[1] De Ming Zhu,[3] Reiza Mukhlis,[3] Jitraporn Vongsvivut,[4] Christopher C. Berndt,[5] Andrew S. M. Ang,[5] and Saulius Juodkazis[1, 6]

[1)] *Optical Sciences Centre and ARC Training Centre in Surface Engineering for Advanced Materials (SEAM), School of Science, Swinburne University of Technology, Hawthorn, Vic 3122, Australia*

[2)] *Australian Research Council (ARC) Industrial Transformation Training Centre in Surface Engineering for Advanced Materials (SEAM), School of Science, Swinburne University of Technology, Hawthorn, Vic 3122, Australia*

[3)] *Swinburne University of Technology, Hawthorn, Vic 3122, Australia*

[4)] *ANSTO-Australian Synchrotron, Infrared Microspectroscopy (IRM) Beamline, 800 Blackburn Road, Clayton, Victoria 3168, Australia*

[5)] *ARC Training Centre in Surface Engineering for Advanced Materials (SEAM), Swinburne University of Technology, Hawthorn, Vic 3122, Australia*

[6)] *WRH Program International Research Frontiers Initiative (IRFI) Tokyo Institute of Technology, Nagatsuta-cho, Midori-ku, Yokohama, Kanagawa 226-8503 Japan*

(Dated: 23 September 2022)

Controlled deposition of $CoCrFeNiMo_{0.2}$ high entropy alloy (HEA) micro-particles was achieved using laser induced forward transfer (LIFT). Ultra-short laser pulses, 230 fs of 515 nm wavelength, were tightly focused into ~ 2.4 μm focal spots on the $\sim$50 nm thick plasma-sputtered films of $CoCrFeNiMo_{0.2}$. The HTA films were transferred onto glass substrates by magnetron sputtering in vacuum (10^{-8} atm) from the thermal spray coated substrates. The absorption coefficient of $CoCrFeNiMo_{0.2}$ $\alpha \approx 6 \times 10^5$ cm^{-1} was determined at 600 nm wavelength. The real and imaginary parts of refractive index $(n + i\kappa)$ of HEA were determined from reflectance and transmittance using nano-films.

Keywords: Laser induced forward transfer, high entropy alloys, micro-particles

CONTENTS

[a)] M.K. and A.M. contributed equally for the laser fabrication and alloy preparation experiments, respectively.
[b)] S.H.N. and A.S.M.A. are the corresponding authors.

I. INTRODUCTION

There is a growing interest in nanostructure studies of nanofilms and nanoparticles in different forms (powder and suspension in liquid). Among them, alloy nanoparticles are especially in the spotlight of nanoscience due to their unique optical and magnetic properties and applications in catalysis, biomedical engineering, and magnetic resonance imaging. High entropy alloys (HEAs)[1] as a novel class of materials have attracted significant attention due to the unique alloy design strategy evolving to random solid solution phase structure, free from any intermetallic compounds[2,3]. Usually, five or more elements including transitional 3d-block and refractory metals are used for the alloy where Mo is found to reduce propensity towards formation of intermetallic compounds[4]. The formation of simple solid solutions grants desirable material properties, such as high thermal stability, strength and ductility combination, and wear and corrosion resistance[5–7]. In addition, HEAs have also exhibited an increased damage resistance to laser irradiation, owing to the effects generated by the rise in configurational entropy, lattice distortion, and compositional complexity[8–10]. Nanoparticles produced by laser ablation as a simple and effective method hold many advantages over chemically produced nanoparticles. Depositing nano-micro-particles by laser induced forward transfer (LIFT) allows patterning over large surfaces and deposition of different materials from different carrier substrates. Among recent LIFT demonstrations are, transfer of bio-materials with low damage of DNA[11], as well as contact deposition for solar cells[12]. Such a particle-on-demand fabrication method can be useful for (photo/electro)-catalysis. The size of nanoparticles made by LIFT are controlled by the diameter of the laser focal spot, its fluence (J/cm^2) and thickness of the nano-film (carrier layer/ink). Typically, nano-films of 10-100 nm thickness are used. Nanofilms of any material can be sputtered or e-beam evaporated into nanolayers, with mixtures formed by varying the number and thickness of multiple layers, for engineering of optical properties (permittivity), as we have shown for plasmonic Olympic Au-Ag-Cu metals[13].

The complex refractive index ($n + i\kappa$) of the HEA nanofilms has to be determined since it solely defines the light-matter characteristics, apart from surface roughness. By measuring the reflectance and transmittance over a wide visible-to-IR spectrum and knowing the thickness of the films, a numerical method of successive approximations can be adopted to determine the complex refractive index of a composite that takes into account the multi-reflections occurring at interface of the target film and the transparent substrate.

The non equi-atomic CoCrFeNiMo$_{0.2}$ HEA shows strong corrosion resistance and stability at ambient temperature. The HEA coatings produced using thermal spray processes are prone to oxidation due to in-flight oxidation. It was found that microparticles smaller than 5 μm in size become oxidised while those larger are only oxidised on the surface in the micro-film coatings[14]. Strong oxidation $\sim$ 50% by atomic numbers was also found in plasma sprayed HEA[15]. However, during the processes of laser ablation and particle formation, changes in temperature might cause precipitation into other phases. Oxidation is also expected to occur. Therefore, the nanoparticles produced are expected to be comprised of multi-phase intermetallic compounds (mainly multi-phase of spinel ferrite nanoparticles) instead of single-phase pure HEA. The structure, morphology, particles size distribution, and chemical composition of the produced nanoparticles is of paramount importance and has to be studied by X-ray diffraction (XRD), scanning electron microscopy (SEM), energy-dispersive spectroscopy (EDS), and Fourier transform (FTIR) and Raman spectroscopies. Additionally, there is a need for controlled deposition of nano/micro-particles of HEAs, which inherit the properties associated with HEA phases without any degradation induced by the LIFT process.

Here, we use LIFT with ultra-short laser pulses which results in the smallest thermal dam-

Preprints (www.preprints.org) | NOT PEER-REVIEWED | Posted: 26 September 2022 doi:10.20944/preprints202209.0392.v1

age to carrier/ink layers due to fast thermal quenching of the transferred material/micro-particle. Optical and structural analysis of nano-films of HEA and their chemical and elemental composition was examined. Optical properties of thin sputtered nano-films of HEA were examined.

II. SAMPLES AND METHODS

High entropy alloy. Commercially available gas atomized (GA) $CoCrFeNiMo_{0.2}$ HEA powder (Jiangsu Vilory, China) with a particle size between 15-53 μm was used as the feedstock to fabricate the HEA coating onto a 3-mm-thick Cu plasma sputtering target backing plate. The $CoCrFeNiMo_{0.2}$ powder was sprayed using a high velocity oxygen fuel (HVOF) thermal spray system (GTV HVOF K2, GTV Verschleißschutz GmbH, Germany). The spray parameters were the following: kerosene fuel at flow rate 28 liters/min, Oxygen flow rate 950 liters/min, a stand-off distance of 380 mm, powder feed rate of 50 g/min, carrier gas was Argon at flow rate of 7 liters/min. The surface of the HEA sputtering targets had a roughness of 1-10 μm (see SEM image in Fig. 1(a)).

Laser induced forward transfer. Femtosecond (fs-)laser microfabrication setup based on Pharos (Light Conversion) fs-laser was integrated with scanning Aerotech xy-stages and software control of laser radiation and scanning conditions (Workshop of Photonics). LIFT mode of micro-particle fabrication was used with HEA-coated glass substrates over the air gap of 10-15 μm determined using imaging with optical microscope. The laser beam was focused through the glass substrate and onto the interface between the HEA film and transparent donor substrate, where the 50 nm HEA film was coated onto the transparent carrier by magnetron sputtering. The transferred HEA droplets were collected by receiving substrates (Si wafer) for further analysis. The laser pulse energy E_p was measured after the objective lens and was used to calculate fluence $F_p = E_p/(\pi r^2)$, where r is the beam waist at the focus. The laser fluences were varied from 5.6 J/cm^2 to 8.9 J/cm^2.

Structural and optical chracterisation. Scanning electron microscopy (SEM) was

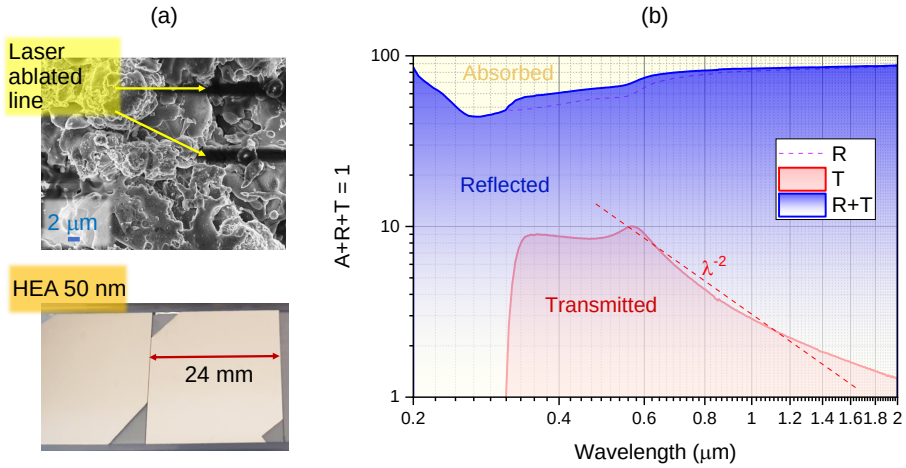

FIG. 1. (a) SEM image of $CoCrFeNiMo_{0.2}$ HEA surface ($\sim$ 100 μm film on Cu-backing plate) with laser ablation trenches. Laser focus was $\sim 1.22\lambda/NA \approx 2.4$ μm for $\lambda = 515$ nm laser wavelength and $NA = 0.26$ objective lens. Photos of HTA $\sim$50 nm film sputtered on cover glass No.4 $\sim$ 0.5 mm (Matsunami). Magnetron sputtering was carried at RF bias power of 100 W rate, 7.5 nm/min deposition rate and 10^{-5} atmosphere pressure (Axxis, JKLesker). (b) Color coded portions of absorbed, A, transmitted, T, and reflected, R, light through the 50-nm-thick sputtered $CoCrFeNiMo_{0.2}$ HEA film. R, T were directly measured using Spectrometer (Lambda 1050 UV/VIS/NIR, PerkinElmer); note logarithmic ordinates scale.

Preprints (www.preprints.org) | NOT PEER-REVIEWED | Posted: 26 September 2022 doi:10.20944/preprints202209.0392.v1

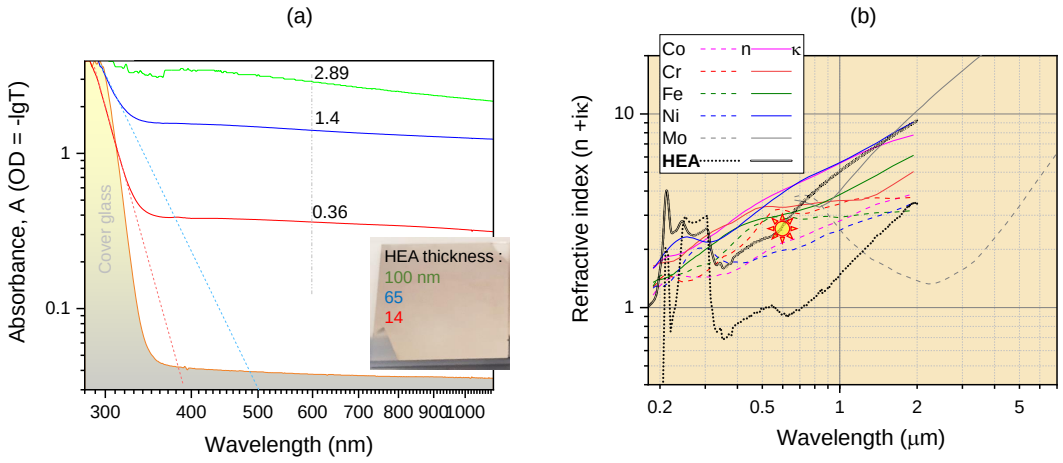

FIG. 2. (a) Absorption spectra of $CoCrFeNiMo_{0.2}$ films of different thickness; cover glass absorption (shaded profile) was compensated using reference (Shimadzu). (b) Real and imaginary parts of the refractive index $(n + i\kappa)$ of the constituent metals and HEA. Marker shows the point of $\kappa = 2.685$ at $\lambda = 600$ nm of the$CoCrFeNiMo_{0.2}$ HEA; absorption coefficient $\alpha = 4\pi/\lambda \approx 6 \times 10^5$ $cm^{-1}$is obtained from the Beer-Lambert law.

used for structural characterisation of samples processed by laser and plasma treatments. Both a 150TWO (Raith) electron beam lithography system used in field-emission SEM mode, as well as a Supra 40VP (Zeiss) equipped with X-ray energy dispersion spectroscopy (EDS) unit (INCA X-act, Oxford instruments Inc.) for elemental analysis was used.

The X-ray photo-electron spectroscopy (XPS) analysis was performed with a Kratos AXIS NOVA spectrometer (Kratos Analytical Ltd, Manchester, UK) using a monochromatized Al-Kα X-ray source (1486.6 eV) operating at a power of 150 W. Survey and high-resolution spectra were acquired at 160 and 20 eV pass energies, respectively (Fig. 5). At least two spots on each sample surface with an elliptical area of approximately 0.3×0.7 mm^2 were analyzed. A charge neutralisation system was employed for effective charge compensation. The vacuum pressure for the XPS analysis was maintained in the order of 10^{-9} Torr. Data analysis and quantification were executed using CASAXPS processing software version 2.3.17 PR 1.1 (Casa Software, Ltd, Teignmouth, UK). The atomic concentrations of each detected element were quantified based on the integral peak intensities and the sensitivity factors provided by the manufacturer. XPS analysis pertains to the thin $\sim$ 10 nm surface bound layer while EDS was contributions from ~ 1 μm depths.

Magnetron sputtering was carried out on an AXXIS physical vapour deposition system (Kurt. J. Lesker). The HEA films with thickness of 14 nm, 65 nm and 100 nm were sputtered onto the 25 mm^2 cover glass. The glass substrates were sonicated in acetone and isopropanol alcohol for 10 minutes each. The power applied to the HEA target was set at 100 W and chamber pressure was 2×10^{-3} Torr, defining the deposition rate of 8.3 nm/min. Before deposition, the pressure of deposition chamber was maintained at a high-vacuum ($\sim 10^{-8}$ Torr) to reduce the effect if oxygen.

Optical characterisation of nanofilms of HEA was carried out with a Lambda 1050 UV/VIS/NIR spectrometer (PerkinElmer). A tungsten halogen lamp is used as the main light source complemented with a Deuterium lamp for shorter wavelengths. A PbS detector and a photomultiplier tube are equipped to detect near-infrared and UV/VIS (860 nm and shorter) wavelengths respectively. Both reflectance R and transmittance T were measured for the three different thickness HEA nanofilms (thickness: 100 nm, 65 nm and 14 nm) over spectra from 175 nm to 2000 nm with a high scanning resolution of 1 nm/scan (UV-1900 Shimadzu). Thickness of films was determined using white light profilometer (ContourGT, Bruker).

Preprints (www.preprints.org) | NOT PEER-REVIEWED | Posted: 26 September 2022 doi:10.20944/preprints202209.0392.v1

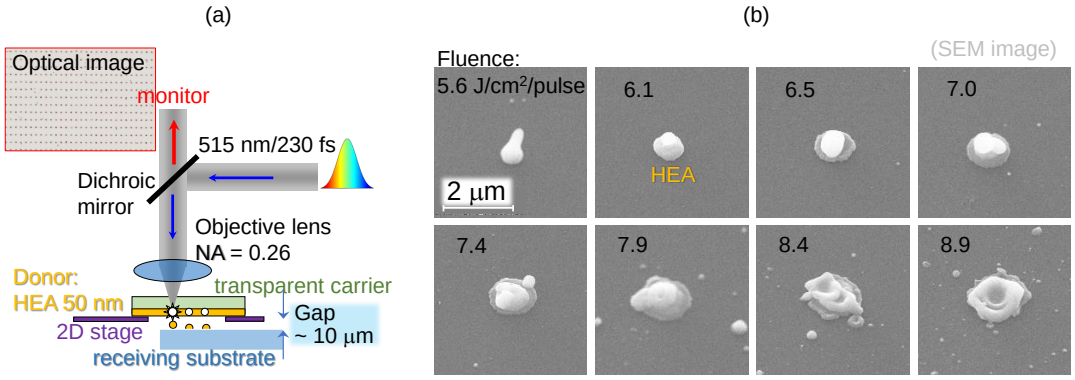

FIG. 3. (a) Laser induced forward transfer (LIFT) of high entropy alloy (HEA) film. (b) SEM images of single sub-1 μm particles of $CoCrFeNiMo_{0.2}$ transferred on a cover glass at different fluences per pulse under $NA = 0.26$ focusing. Laser irradiation: 230 fs, 515 nm. Thickness of HEA was 50 nm.

Numerical modeling. Three-dimensional (3D) finite-difference time-domain (FDTD) simulation was performed using commercial software (FDTD solution, Lumerical Inc.). The snowman-like micro-particle shape was simplified as a combination of a bottom sphere (diameter: 500 nm) and a top spheroid (semi-major diameter: 500 nm; semi-minor diameter: 250 nm). The HEA material was defined by the calculated complex refractive index $(n+i\kappa)$ over the spectrum range from 175 nm to 2000 nm.

III. RESULTS AND DISCUSSION

Non equi-atomic $CoCrFeNiMo_{0.2}$ high entropy alloy (HEA) nanofilms were prepared by physical vapor deposition (PVD) in vacuum from ~ 100 μm coatings made on the plasma sputtering targets by the HVOF process (Sec. II). Then HEA nano-/micro-particles were made by light-induced forward transfer (LIFT) using ablation of HEA nano-films irradiated by single femtosecond laser pulses.

A. Optical characterisation of HEA nano-films: (n, κ)

By measuring R and T for an HEA film on known thickness (strongly absorbing) on a transparent substrate, the complex refractive index $(n + i\kappa)$ of the HEA nanofilms can be determined[16] by using following equation used for Pd-Au alloys[17]:

$$R = \frac{(1-n_1)^2+\kappa_1^2}{(1+n_1)^2+\kappa_1^2}; \quad T = \frac{16n_2(n_1^2+\kappa_1^2)}{[(n_1+n_2)^2+(\kappa_1+\kappa_2)^2][(1+n_1)^2+\kappa_1^2]} e^{\frac{-4\pi d}{\lambda}}, \qquad (1)$$

where the n_1, κ_1, n_2, and κ_2 are the real and imaginary parts of the complex refractive index of HEA film and cover glass, respectively, R and T are the overall reflectance and transmittance at the normal incidence, d is the thickness of the HEA film, and the λ is the wavelength. Figure 1(b) shows experimentally measured R and T presented as fractions of transmitted, reflected and absorbed portions of incident light. This was used for the calculation of (n, κ) using Eqn. 1 with thickness d determined by optical profilometer. Figure 2 shows Beer-Lambert absorbance of different thickness of HEA films on cover glass (a) and (n, κ) data for the constituent metals and the HEA film (from the data shown in Fig. 2(b)). Interestingly, a sub $n < 1$ refractive index was observed at visible wavelengths. This is is promising for engineering of epsilon-near-zero (ENZ) materials with permittivity

Preprints (www.preprints.org) | NOT PEER-REVIEWED | Posted: 26 September 2022 doi:10.20944/preprints202209.0392.v1

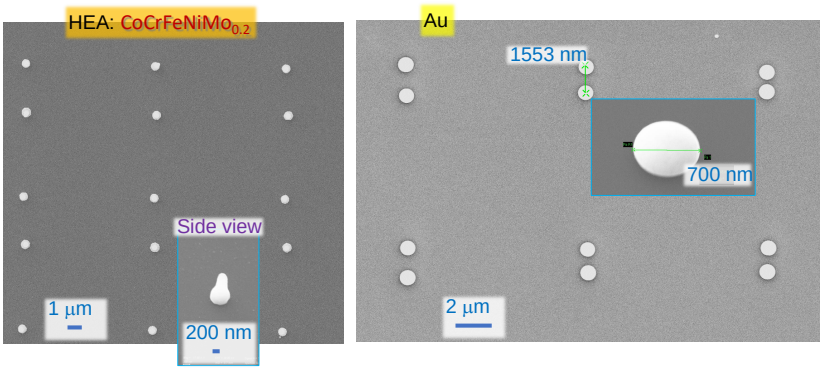

FIG. 4. Arrays of micro-particles made by LIFT of high of $CoCrFeNiMo_{0.2}$ and Au; transferred onto Si wafer at pulse energies $E_p = 344$ nJ or 5.6 J/cm^2 (on sample) for HEA and 816 nJ or 14 J/cm^2 for Au under $NA = 0.26$ focusing. Laser irradiation: 230 fs, 515 nm. Thickness of HEA and Au was 50 nm.

("epsilon") $\varepsilon = (n+i\kappa)^2$, which are used in perfect absorbers[18]. The free-carrier absorption can be recognised by $\kappa \propto \lambda^2$ for $\lambda > 0.6$ μm.

B. Micro-particles and their arrays out of HEA

HTA films made by thermal spray are micro-rough (Fig. 1(a)) and were plasma sputtered into 50 nm films on glass substrates for characterisation as well as for LIFT. Figure 1(b) shows color-coded portions of absorbed A, transmitted T and reflected R light comprising the energy conservation by $A + R + T = 100\%$ (note the log-log scale of the spectrum). Only $\sim 10\%$ of light is transmitted over the visible part of spectrum 400-800 nm. This is typical for metal coatings where $1/e^2$-level of transmitted power/intensity, the skin depth $1/\alpha$, is tens-of-nm for the absorption coefficient $\alpha = 4\pi\kappa/\lambda$. From around $\lambda = 600$ nm, transmittance drops at longer wavelengths. That is typical for free carrier absorption, which increases as $\propto \lambda^2$ (see dashed line with slope of -2). The portion of reflected light increases with λ, while transmission decreases for the same reason, the high free carrier density. This defines a smaller portion of light absorbed at the IR spectral window where the 50 nm HEA film becomes negligibly thin.

Absorption coefficient α was determined from direct measurement of transmittance using uncoated glass reference (No. 4 Matsunami cover glass) in the reference arm of spectrometer (Shimazu) for different thicknesses of HEA coating; the glass substrate contribution is canceled in the plotted spectra (Fig. 2(a)). Thickness of deposited HEA film was calibrated using an optical profilometer; a 7.5 nm/min deposition rate of film was used. The extinction coefficient of the HEA film was $\kappa = 2.685$ which yields $\alpha = 6 \times 10^5$ cm^{-1} absorption coefficient (at the 600 nm wavelength selected). This value is consistent with extinction of the metals used in the alloy (Fig. 2(b)).

The established strong absorption of HEA nanofilms (Fig. 2) is defined by the optical density $OD \approx 1$ with transmitted intensity $I_t = I_{in}10^{-OD} \equiv e^{-\alpha d}$ for the thickness d. For fs-laser LIFT we used 515 nm wavelength, which is in this strongly absorbing range. The energy of the laser pulse is deposited into the skin depth, which closely matches the thickness of the HTA film. The forward momentum of laser pulse is cumulative of single photon momenta $p = h/\lambda$, where h is the Plank's constant, and is deposited by absorption. The laser beam energy is linked to the momentum via $E = pc$, c is speed of light. In case of reflection, double the large momentum is deposited due to the change in direction of light upon reflection. The melted and pushed droplet from the carrier/ink layer is transferred onto the receiving substrate.

Preprints (www.preprints.org) | NOT PEER-REVIEWED | Posted: 26 September 2022 doi:10.20944/preprints202209.0392.v1

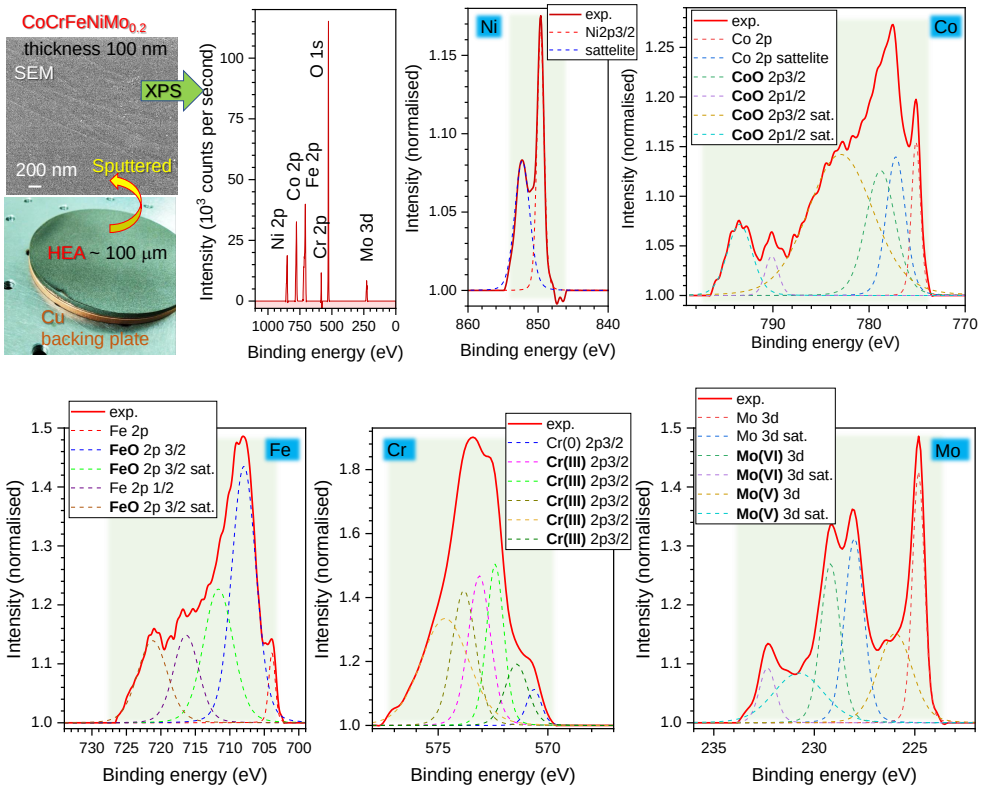

FIG. 5. X-ray photo-electron spectroscopy (XPS) of $CoCrFeNiMo_{0.2}$ 100-nm-thick film transferred on a cover glass by magnetron sputtering. Such a film was used as as a carrier for LIFT. Magnetron sputtering was carried out at the order of 10^{-3} Torr. CasaXPS software package was used for XPS data analysis. A wide range binding energy spectrum and detailed elemental bands (normalised) are shown; background-highlights (green) show the energy window used for quantification. Bold markers in the legends are for the oxide states: CoO, FeO, Cr(III) [chromia Cr_2O_3], Mo(VI) [MoO_3] and Mo(V) [Mo_2O_5].

We used a spacing of $\sim$ 10 μm between the carrier and receiver as was judged from observation in an optical microscope (Fig. 3(a); height control $\sim$ 1 μm). A fairly narrow fabrication window of fluence 5-6 J/cm^2/pulse exists for LIFT for the most uniform particles. When the laser fluence was just above the ablation threshold, droplet-shape micro-particles with a size smaller than the laser spot size were transferred by LIFT. As the laser fluence increased, the shape of the micro-particles evolve from snowman-like to multilayer pancake-like. At high fluences, the transferred micro-particles were approximately the same as the laser spot size with many debris around.

With the proper choice of pule energy/fluence, it was possible to transfer uniform HEA sub-1 μm particles onto any receiving substrate (Fig. 4). For comparison, gold micro-particles transferred by LIFT can be larger when larger pulse fluence is used, however, for HEA such irradiance would cause loss of shape and size.

C. Material characterisation

The XRD patterns for a gas-atomized $CoCrFeNiMo_{0.2}$ powder and HVOF $CoCrFeNiMo_{0.2}$ coating are illustrated in Fig. 7(a). The phase composition of the powder is primarily a single solid solution based on face centered cubic (FCC) phase structure, which was retained

 doi:10.20944/preprints202209.0392.v1

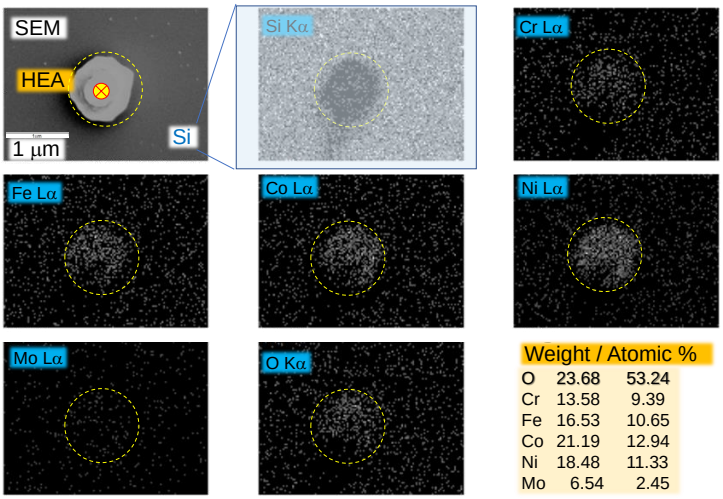

FIG. 6. X-ray energy-dispersive spectroscopy (EDS) mapping of a microparticle of $CoCrFeNiMo_{0.2}$ on Si substrate (Oxford on Zeiss SEM microscope).

in the coating produced using HVOF without indicating any peaks relating to oxides or intermetallic compounds. The higher magnification back-scattered electron (BSE) SEM micrograph of HVOF coating shown in Fig. 7(b) revealed inter-splat regions and randomly dispersed pores without any substantial depth variation within the microstructure of the coating. In addition, minor oxide fragments across the inter-splat regions were identified with an average chemical composition of 25.2 at% O, 17.2 at% Co, 18.7 at% Cr, 19.4 at% Fe, 15.9 at% Ni and 3.6 at% Mo when measured using point EDS analysis. Therefore, the composition of the oxides is attributed to the spinel-based oxide structure, which was developed due to the in-flight oxidation characteristics of the HVOF process. More importantly, the absence of oxide peaks in the XRD diffractogram of the $CoCrFeNiMo_{0.2}$ coating signified their relatively low concentration across the microstructure. The oxygen rich regions were only observed by XPS, which is surface sensitive and is discussed below.

With several processing steps involved from thermal spray, Ar-ion plasma sputtering to micro-particle formation by laser ablation, it is important to establish chemical changes. Laser ablation is taking place with electron excitation and departure from the surface. In chemistry terms, this is oxidation (loss of an electron). Ar-ion sputtering of HEA films which are composed of squashed micro-droplets of tens-of-μm can have preferential sputtering of the interfaces and boundaries. The fs-laser ablation and LIFT is very non-equilibrium process and formation of different phases of materials is possible due to highly dynamic ion separation governed by difference in the ion masses[19,20].

To characterise the target source used for the LIFT printing of single micro-droplets of HEA, XPS analysis of 100-nm-thick sputtered films was carried out (Fig. 5). Presence of oxides was most pronounced for CoO, FeO, chromia Cr_2O_3, and MoO_3; oxides shows on the higher binding energy side (Fig. 5). Qualitatively similar results for HEA prepared by thermal and plasma spray were observed[14,15]. High-vacuum (10^{-8} Torr) sputtering of HEA targets onto glass was not expected to contribute to a larger portion of oxides in the film. However, some surface oxidation of the HEA nano-film on glass is expected at room conditions after deposition, e.g., this was observed for Cr coating. Noteworthy, the oxide surface layer is on the far-side from the glass-HEA film interface with is irradiated for LIFT. Hence, fs-laser pulse interacts mostly with the less oxidised part of the HEA film.

Since HEA targets were made using thermal spray, there was carbon presence in the film as well. The ratio of O 1s to C 1s peaks was 43.38%:38.21% and 42.08:38.77% in two different samples. The ratio of Oxygen to all the metals (Ni, Co, Fe, Cr, Mo) was: 70.21% to (3.19-Ni; 7.91-Co; 11.18-Fe; 5.63-Cr; 1.88%-Mo) and 68.72% to (3.97-Ni; 7.69-Co; 12.12-Fe;

Preprints (www.preprints.org) | NOT PEER-REVIEWED | Posted: 26 September 2022 doi:10.20944/preprints202209.0392.v1

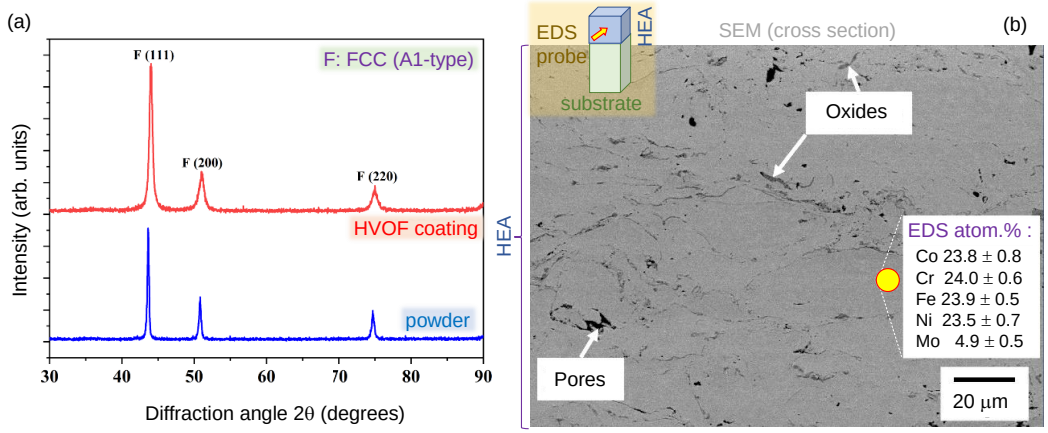

FIG. 7. Thick HEA film deposited by high temperature spray. (a) X-ray diffraction (XRD) of diffractograms of gas atomized $CoCrFeNiMo_{0.2}$ powder and HVOF sprayed coating (GTV HVOF K2, GTV Verschleißschutz GmbH, Germany). (b) The cross-sectional scanning electron microscopy (SEM) image of HVOF $CoCrFeNiMo_{0.2}$ coating along with EDS analysis of the coating phase in atomic percentage.

5.57-Cr; 1.91%-Mo) in the very same samples/areas (Fig. 5). Composition differences were not expected between those two areas/samples and are caused solely by uncertainties. If carbon is added for 100% composition of the samples, one would find the following atomic ratios [%]: 43.38(O), 38.21(C) and for metals 1.97-Ni, 4.89-Co, 6.91-Fe, 3.48-Cr, 1.16-Mo (sample No. 1); 42.08(O), 38.77(c) and 2.43-Ni, 4.71-Co, 7.42-Fe, 3.41-Cr, 1.17-Mo (sample No. 2).

The elemental composition of single micro-particles of HEA printed by LIFT was characterised using EDS (Fig. 6). LIFT was carried out onto a Si substrate and oxygen contribution from the substrate's native oxide ($\sim$ 2 nm) is minimal, since EDS probes the deep sub-surface volume at $\sim$ 1 μm depth, in contrast to the surface bound (nanometres) XPS. Oxidation of microdroplets (on Si) was smaller as compared with XPS data of the nano-film used for laser printing (Fig. 5) judging from the O-atomic content of selected micro-particle reaching $\sim$ 53% atomic (here, C was not used for the quantification and it was negligible in the spectral survey, most probably due to oxidation during LIFT). This is consistent with XPS data for the HEA film on glass, which was used as a source for droplet transfer. The reference EDS results of sub-mm HEA film measured into the film (side view SEM) is shown in Fig. 7 together with X-ray diffraction results.

The comparative EDS analysis between target coating and particle revealed significant difference with the chemical composition. The oxygen content within the particle increases significantly as compared to the target due to the high temperature involved in the LIFT process. The substantial decrease in elemental content of Co, Cr, Fe and Ni attributed to equatorial proneness of these elements towards the oxidation. By using high-temperature melting substrates such as crystalline Al_2O_3, it is possible to prepare HEA nano-ink films for LIFT (Fig. S3). Also, thermal remelting of sputtered HEA can be used to produce alloys of better crystalline quality. Even a strategy to sputter 2-5 nm films of separate metals on a pre-heated substrate or to anneal films afterwards is another avenue to produce HEA and need to be investigated since it was found to work for Pd-Au alloy[17].

IV. CONCLUSIONS AND OUTLOOK

It was shown that films of tens-of-nm thickness had optical properties closely matching those of metals with absorption coefficient corresponding to the strong absorbance $\alpha \approx 5 \times 10^5$ cm^{-1} in the visible spectral range. Strong reflectance in the near-IR region is also

consistent with free-carrier (electron) absorption $\alpha \propto \kappa \propto \lambda^2$ at longer wavelengths (as expected for metals). Direct laser writing of single sub-1 μm particles and their arrays was demonstrated in a single pulse mode for focusing into a ~ 2.4 μm spot.

Future studies of HEA oxidation during LIFT can be carried out using synchrotron IR micro-spectroscopy since metal oxides have absorption bands over the fingerprinting IR region. Also, formation of metallic glass phases is expected due to fast thermal quenching using fs-laser LIFT. High-resolution X-ray and neutron scattering techniques are promising to reveal further details on composition and morphology.

ACKNOWLEDGMENTS

We are grateful to Workshop of Photonics Ltd., Lithuania for fs-laser fabrication setup acquired via a technology transfer project in 2012. This study was supported by the Australian Research Council (ARC) under the Industrial Transformation Training Centre project IC180100005 that is titled "Surface Engineering for Advanced Materials", SEAM. We are grateful for the additional support for the industrial, university and other organization partners who have contributed to the establishment and support of SEAM. Financial support via ARC Linkage LP190100505 and the ARC Discovery DP190103284 projects is acknowledged. The beamtime EU18414 at the IR micro-spectroscopy beamlime at the Australian Synchrotron was used for IR reflectivity measurements.

[1] J.-W. Yeh, Y.-L. Chen, S.-J. Lin, and S.-K. Chen, "High-entropy alloys – a new era of exploitation," Materials Science Forum. **560**, 1–90 (2007).

[2] J.-W. Yeh, S.-J. Lin, T.-S. Chin, J.-Y. Gan, S.-K. Chen, T.-T. Shun, C.-H. Tsau, and S.-Y. Chou, "Formation of simple crystal structures in Cu-Co-Ni-Cr-Al-Fe-Ti-V alloys with multi-principal metallic elements," Metallurgical Materials Transactions A **35**, 2533–2536 (2004).

[3] J.-W. Yeh, S.-K. Chen, S.-J. Lin, J.-Y. Gan, T.-S. Chin, T.-T. Shun, C.-H. Tsau, and S.-Y. Chang, "Nanostructured high-entropy alloys with multiple principal elements: Novel alloy design concepts and outcomes," Adv. Eng. Mat. **6**, 299–303 (2004).

[4] T. Whitfield, E. Pickering, L. Owen, O. Senkov, D. Miracle, H. Stone, and N. Jones, "An assessment of the thermal stability of refractory high entropy superalloys," J. Alloys Compounds **857**, 157583 (2021).

[5] W. Li, D. Xi, D. Li, Y. Zhan, Y. Gao, and P. Liaw, "Mechanical behavior of high-entropy alloys," Progress Mat. Sci. **118**, 100777 (2021).

[6] R. K. Nutor, Q. Cao, X. Wang, D. Zhang, Y. Fang, Y. Zhang, and J.-Z. Jiang, "Phase selection, lattice distortions, and mechanical properties in high-entropy alloys," Adv. Eng. Mat. **22**, 2000466 (2020).

[7] A. Meghwal, A. Anupam, B. Murty, C. Berndt, R. Kottada, and A. Ang, "Thermal spray high-entropy alloy coatings: A review," J. Thermal Spray Technol. **29**, 857–893 (2020).

[8] Q. Xu, H. Q. Guan, Z. H. Zhong, S. S. Huang, and J. J. Zhao, "Irradiation resistance mechanism of the CoCrFeMnNi equiatomic high-entropy alloy," Scientific Reports **11**, 608 (2021).

[9] Y. Lin, T. Yang, L. Lang, C. Shan, H. Deng, W. Hu, and F. Gao, "Enhanced radiation tolerance of the Ni-Co-Cr-Fe high-entropy alloy as revealed from primary damage," Acta Materialia **196**, 133–143 (2020).

[10] C. Lua, T. Yang, K. Jin, N. Gao, P. Xiu, Y. Zhang, F. Gao, H. Bei, W. Weber, K. Sun, Y. Dong, and L. Wang, "Radiation-induced segregation on defect clusters in single-phase concentrated solid-solution alloys," Acta Materialia **127**, 98–107 (2017).

[11] P. Karakaidos, C. Kryou, N. Simigdala, A. Klinakis, and I. Zergioti, "Laser bioprinting of cells using uv and visible wavelengths: A comparative DNA damage study," Bioengineering **9**, 378 (2022).

[12] S. Pozov, K. Andritsos, I. Theodorakos, E. Georgiou, A. Ioakeimidis, and I. Zergioti, "Indium tin oxide-free inverted organic photovoltaics using laser-induced forward transfer silver nanoparticle embedded metal grids," ACS Applied Electronic Materials **4**, 2689–2698 (2022).

[13] Y. Hashimoto, G. Seniutinas, A. Balčytis, S. Juodkazis, and Y. Nishijima, "Au-Ag-Cu nano-alloys: tailoring of permittivity," Sci. Reports **6**, 25010 (2016).

[14] A. Anupam, R. S. Kottada, S. Kashyap, A. Meghwal, B. Murty, C. Berndt, and A. Ang, "Understanding the microstructural evolution of high entropy alloy coatings manufactured by atmospheric plasma spray processing," Applied Surface Science **505**, 144117 (2020).

[15] A. Meghwal, A. A. andcV Luzin, C. Schulz, C. Hall, B. Murty, R. S. K. andC C Berndt, and A. S. M. Ang, "Multiscale mechanical performance and corrosion behaviour of plasma sprayed AlCoCrFeNi high-entropy alloy coatings," J Alloys Compounds **854**, 157140 (2021).

[16] J. Avila, R. Matelon, R. Trabol, M. Favre, D. Lederman, U. Volkmann, and A. Cabrera, "Optical properties of Pd thin films exposed to hydrogen studied by transmittance and reflectance spectroscopy," J. Appl. Phys. **107**, 023504 (2010).

[17] Y. Nishijima, S. Shimizu, K. Kurihara, Y. Hashimoto, H. Takahashi, A. Balcytis, G. Seniutinas, S. Okazaki, J. Juodkazyte, T. Iwasa, T. Taketsugu, Y. Tominaga, and S. Juodkazis, "Optical readout of hydrogen storage in films of Au and Pd," Opt. Express **20**, 24081–24092 (2017).

[18] Y. Nishijima, N. To, A. Balcytis, and S. Juodkazis, "Absorption and scattering in perfect thermal radiation absorber-emitter metasurfaces," Optics Express **30**, 4058–4070 (2022).
[19] S. Juodkazis, K. Nishimura, S. Tanaka, H. Misawa, E. E. Gamaly, B. Luther-Davies, L. Hallo, P. Nicolai, and V. Tikhonchuk, "Laser-induced microexplosion confined in the bulk of a sapphire crystal: Evidence of multimegabar pressures," Phys. Rev. Lett. **96**, 166101 (2006).
[20] A. Vailionis, E. G. Gamaly, V. Mizeikis, W. Yang, A. Rode, and S. Juodkazis, "Evidence of super-dense Aluminum synthesized by ultra-fast micro-explosion," Nature Communications **2**, 445 (2011).
[21] J. Lapidas, A. Zhizhchenko, E. Pustovalov, D. Storozhenko, and A. Kuchmizhak, "Direct laser printing of high-resolution physically unclonable function anti-counterfeit labels," Appl. Phys. Lett. **120**, 261104 (2022).

Preprints (www.preprints.org) | NOT PEER-REVIEWED | Posted: 26 September 2022 doi:10.20944/preprints202209.0392.v1

Appendix A: Light-field enhancement by Au micro-particle at IR wavelengths

Samples of Au micro-particles were patterned on Si (Fig. S1(a); similar as in Fig. 4) for mapping of reflectance R at selected wavenumbers $\tilde{\nu}$ at two perpendicular polarisations (at the IR micro-spectroscopy beamline of the Australian Synchrotron). Example of R map at $\tilde{\nu} = 2800$ cm^{-1} ($\lambda = 3.57$ μm) is shown in Fig. S1(b). Slight light E-field enhancement is observed in reflection from regions between sub-1 μm Au spheres (aligned in pairs along x-direction (a)) for the horizontal x-pol. This corresponds to the alignment direction of micro-particles in the pair. Separation between two microparticles was ~ 3 μm and it was sub-wavelength for the used mapping wavelength of $\lambda = 3.57$ μm. Stronger reflectivity is expected from Au micro-sphere and due to light concentration on the pair of Au micro-spheres.

At perpendicular (y-pol.), a small enhancement was observed at position of the pair of Au microparticles rather in between the lines; noteworthym that separation between the lines of paired Au microparticles was larger by approximately the gap between them in x-direction. There was strong edge effects at the extremities of read-field. Mapping was made using a point MCT detector. Synchrotron radiation has a complex polarisation distribution due to beam extraction from the synchrotron by mirror with a gap at its center (the 1st fork-mirror) and direction of observation. This usually cause not even intensity across the focus which contributes to unevenness of intensity maps on 3D sturfaces.

Appendix B: Light enhancement by micro-particle of HEA

Light field enhancement by a single HEA micro-particle: sphrere and snowman were modeled using FDTD at different wavelengths through visible to near-IR spectral range (Fig. S2). The experimentally determined spectral dependence of n, κ was used for the modeling (Fig. 2(b)). Expected light field localisation by metallic nanoparticle was observed with most of light concentration and enhancement taking place around a metallic nanoparticle. Such nano-/micro-particles can be used for surface enhance Raman scattering (SERS) sensors as well as color markers[21].

The phase change of the reflected field E_r (in air) from the surface with refractive index n is defined by $E_r = -\frac{n-1}{n+1}E_{in}$, where E_i is the incident E-field; the minus sign means the opposite phase or the π-shift. When $n > 1$, there is a π-shift between the incident and reflected E-fields of light while for the $n < 1$, there is no phase change between E_r and E_i. The latter situation can be realised at the visible spectral range where $n < 1$ for HEA (see, $\lambda = 600$ nm case in Fig. S2).

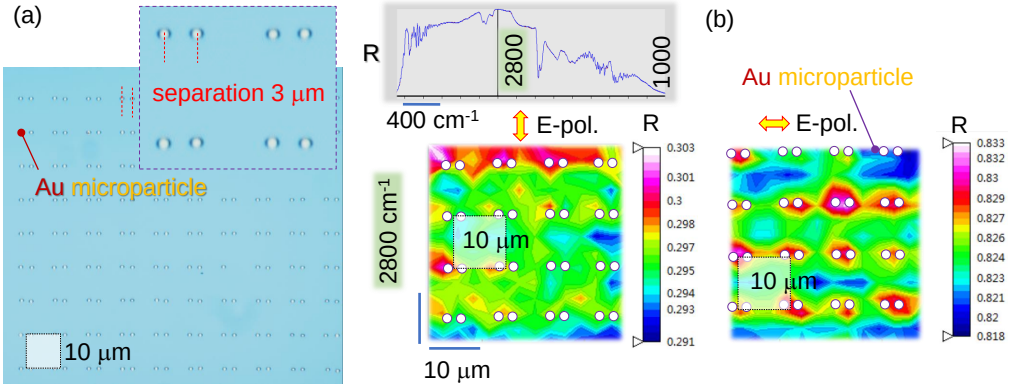

FIG. S1. (a) Optical image (reflection) of Au micro-particles on Si substrate. (b) Reflection spectral mapping of Au micro-particles (pairs) patterned at $\Lambda_{x,y} = 10$ μm array at two perpendicular polarisations; map taken at 2800 cm^{-1} or 3.57 μm or 83.94 THz. Circular markers are locations of Au microparticles of ~ 0.7 μm. Au microparticled were LIFT transferred from 50 nm film using $NA = 0.26$ objective lens at pulse energy $E_p = 816$ nJ. Separation between Au microparticles 3 μm. Light source is Australian Synchrotron. Mapping was carried out by MCT detector scanning pinhole aperture was 3 μm. Reference was flat Si substrate.

Preprints (www.preprints.org) | NOT PEER-REVIEWED | Posted: 26 September 2022 doi:10.20944/preprints202209.0392.v1

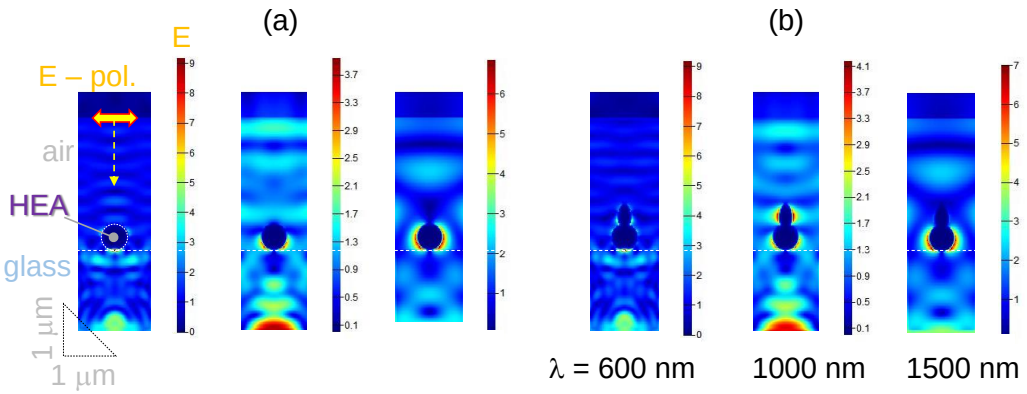

FIG. S2. Light field enhancement by a HEA micro-particle (on glass) at different wavelengths calculated by FDTD for spherical (a) and snow-man (b) structures as observed in experiments (Fig. 3(b)); incident E-field is $|E| = 1$. HEA is modeled as homogeneous refractive index $(n + i\kappa)$ of HEA (Fig. 2(b)). Boundary conditions: perfect matching layer.

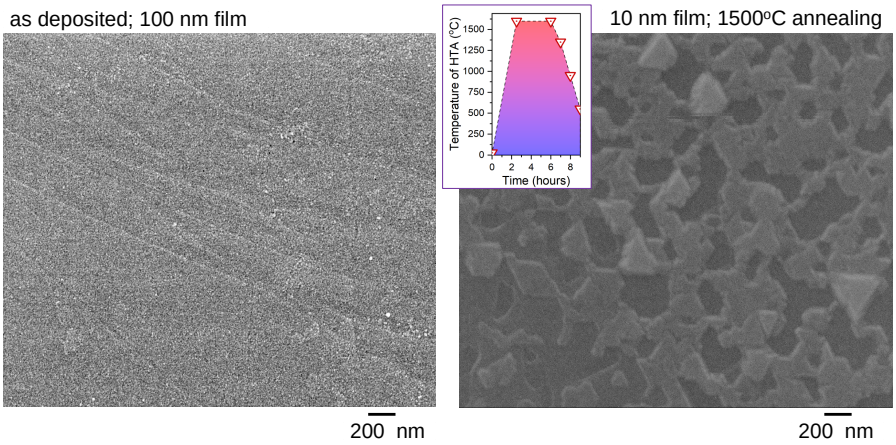

FIG. S3. SEM images of the as sputtered $CoCrFeNiMo_{0.2}$ film and after high temperature annealing at 1500°C for 2 hours under N_2 flow to avoid oxidation. Substrate was Al_2O_3 crystalline substrate with c-plane used for deposition of HEA (sapphire melts at $\sim$ 2100°C). For SEM imaging of the annealed sample 10 nm of Cr was coated to reduce charging.

Appendix C: High temperature annealing of HEA

Another possible technique for fabrication of nano-/micro-particles is the high temperature dewetting of nano-thin films. For example 20 nm of Au on fused silica SiO_2 substrate can be transformed into nano-islands by 650°C annealing for 1 hour. Thin 10 nm $CoCrFeNiMo_{0.2}$ film was sputtered on crystalline Al_2O_3 substrate and annealed at high 1500°C temperature for possible dewetting (Fig. S3). Surface morphology was obviously changed from nano-smooth initial HEA film revealing structures of 100-300 nm in lateral cross sections after HTA (see HTA protocol in the inset of Fig. S3) under SEM observation. Further studies will be carried out for structural and chemical composition of the film. Also, sublimation of HEA is another important phenomenon which needs to be investigated by HTA.